Available online at www.sciencedirect.com
SCIENCE DIRECT®
Sensors and Actuators A 105 (2003) 271–285
SENSORS AND ACTUATORS A PHYSICAL
www.elsevier.com/locate/sna

Some new horizons in magnetic sensing: high-T_c SQUIDs, GMR and GMI materials

A.E. Mahdi [a,*], L. Panina [b,1], D. Mapps [b,2]

[a] *Department of Electronic and Computer Engineering, University of Limerick, Plassey Technological Park, Limerick, Ireland*
[b] *Department of Communication and Electrical Engineering, University of Plymouth, Plymouth, Devon PL4 8AA, UK*

Received 3 April 2003; received in revised form 3 April 2003; accepted 8 April 2003

Abstract

Driven by rapid progress in microelectronics and thin film technologies, magnetic sensors development continues to expand. This paper presents issues related to the principles, categorisation and applications of magnetic sensors. Special attention is paid to two types of sensors and their present and future impact: superconducting quantum interference devices (SQUID) magnetometers with their unsurpassed sensitivity, and giant magnetoresistance (GMR)/giant magnetoimpedance (GMI) based sensors as the most promising technology. A review of recent developments in SQUID technology and a discussion of limitations and aspects that could contribute to the wider acceptance of this technology, are presented. The giant magnetoresistance and giant magnetoimpedance effects have already found applications in magnetic sensing and have promise in other applications. Their unique characteristics and miniaturisation potential have contributed to the rapid acceptance of these technologies. The article describes the principles of the GMR and GMI effects along with recent developments in these technologies particularly in manufacturing techniques and materials.

Keywords: Magnetic sensors; SQUID; GMR; GMI

1. Introduction

Magnetic sensors have been of great assistance to mankind in a variety of applications, ranging from suspended magnets used for navigation to small thin film detectors which sense information in the form of magnetic reversals on computer disks. For most applications, magnetic sensors offer safe, non-invasive, non-destructive means of detection, and provide a more rugged, reliable and maintenance-free technology compared to other sensor technologies.

Magnetic sensing techniques exploit a broad range of physics and chemistry concepts, most of which based on the intimate connection between magnetic and electric phenomena, such as Lorentz force, Faraday rotation, Hall effect and other galvanomagnetic effects. Though the basic underlying physics remain the same, today all these basic measurements are carried out with ever increasing finesse. For example, superconducting quantum interference devices (SQUIDs) are used for very accurate measurements of the earth's magnetic field. State-of-the-art semiconductor fabrication techniques coupled with modern micromachining techniques have facilitated new types of solid-state, thick and thin film magnetic sensors and related transducers that offer solutions to many drawbacks normally associated with similar structures at larger scales [1]. In the first part of this paper, the concepts and operational principles of major magnetic sensor technologies will be described. The second part of the paper is dictated by a review of the theory, applications, and recent developments in SQUID magnetometer, GMR and GMI based sensor technologies.

2. Magnetic sensor technologies

A magnetic sensor is a transducer that converts a magnetic field into an electrical signal. In general, the operational principle is based on either dc or ac technology. Fig. 1 shows a family tree of some magnetic sensors materials and effects.

2.1. Physical and operational principles of magnetic sensors

Most magnetic sensors that use dc excitation are based on exploitation of galvanomagnetic effects due to the Lorentz

* Corresponding author. Tel.: +353-61-213492; fax: +353-61-338176.
E-mail addresses: hussain.mahdi@ul.ie (A.E. Mahdi), lpanina@plymouth.ac.uk (L. Panina), dmapps@plymouth.ac.uk (D. Mapps).
[1] Tel.: +44-1752-232604; fax: +44-1752-232583.
[2] Tel.: +44-1752-232570; fax: +44-1752-232583.

0924-4247/$ – see front matter © 2003 Elsevier B.V. All rights reserved.
doi:10.1016/S0924-4247(03)00106-7

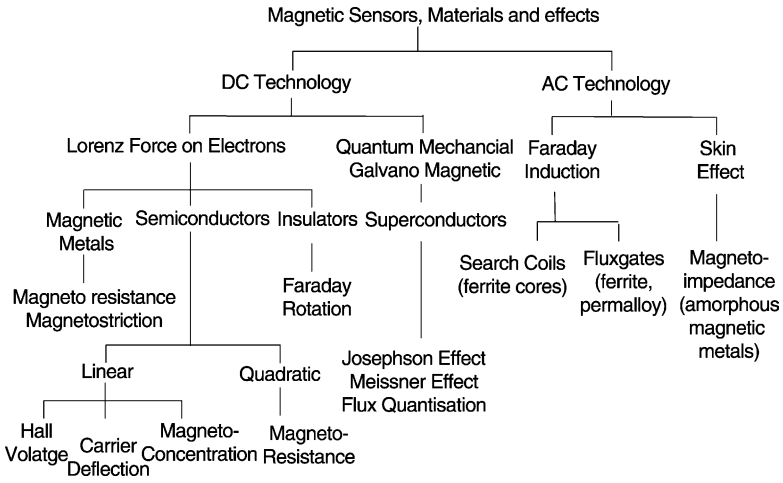

Fig. 1. Family tree of magnetic sensor materials and effects.

force on moving electrons in a metal, semiconductors, or an insulator in one way or another. These effects occur when a material carrying an electric current is exposed to a magnetic field. The best-known fundamental galvanomagnetic effects are the Hall effect, which produces an electric field perpendicular to the magnetic induction vector and the original current direction, and the magnetoresistive effect, which is the increase in material resistivity due to exposure to the magnetic field [1]. Other galvanomagnetic effects include the quantum mechanical galvanomagnetic effects occurring in Josephson junctions between superconducting materials [2].

Generally, galvanomagnetic effects are manifestations of the charge-carrier transport phenomena occurring in matters when the carriers are subject to the action of the Lorentz force $\boldsymbol{F}$:

$$\boldsymbol{F} = e\boldsymbol{E} + e[\boldsymbol{v} \times \boldsymbol{B}] \tag{1}$$

where e denotes the carrier charge (for electrons $e = -q$, and for holes $e = q$ and $q = 1.6 \times 10^{-19}$ C), $\boldsymbol{E}$ denotes the electric field, $\boldsymbol{v}$ the carrier velocity and $\boldsymbol{B}$ the magnetic induction. The first term on the right-hand side of Eq. (1) represents a Coulomb force and the second term is the Lorentz force law. For nondegenerate semiconductors exposed to transverse electrical and magnetic fields (i.e. $\boldsymbol{E} \cdot \boldsymbol{B} = 0$), the current transport equation for one type of carrier becomes [3]:

$$\boldsymbol{J} = \boldsymbol{J}_0 + \mu_{\mathrm{H}}[\boldsymbol{J}_0 \times \boldsymbol{B}] \tag{2}$$

where $\boldsymbol{J}$ denotes the total current density and the term $\boldsymbol{J}_0 = \sigma\boldsymbol{E} - eD\nabla n$ is the current density due to only the electric field and carrier-concentration gradient ∇n. However, $\boldsymbol{J}_0 \neq \boldsymbol{J}(\boldsymbol{B} = 0)$, since a magnetic field generally influence the electric potential and carrier-concentration distributions. The transport coefficients μ_{H} (the Hall mobility which has the sign of the corresponding charge-carrier), σ (the conductivity), and D (the diffusion coefficient) are determined by the carrier scattering processes and generally depend on electric and magnetic fields. Both the Hall and the magnetoresistive effects can be derived from the solutions of Eq. (2) subject to the appropriate boundary conditions.

The Hall effect in semiconductors is best understood by considering a special case of carrier transport in a very long strip with narrow cross-section of a strongly extrinsic and homogeneous ($\nabla n = 0$) semiconductor material, subjected to a magnetic field described by a magnetic flux density $\boldsymbol{B} = (0, B_y, 0)$. Assuming that the strip axis is along the x-axis, and the strip plane is the xz-plane, then if the strip is exposed to an external electric field $\boldsymbol{E}_{\mathrm{ex}} = (E_x, 0, 0)$, a current $\boldsymbol{I}$ will flow through it with current density $\boldsymbol{J} = (J_x, 0, 0)$. Since $J_z = 0$, an internal transverse electric field $\boldsymbol{E}_{\mathrm{H}}$ must build up in order to counteract the 'magnetic' part of Lorentz force (the second term in Eq. (1)). The field $\boldsymbol{E}_{\mathrm{H}}$ is known as the Hall field and can be determined from Eq. (2) by substituting $\boldsymbol{E} = \boldsymbol{E}_{\mathrm{ex}} + \boldsymbol{E}_{\mathrm{H}}$, under the condition that the transverse current density vanishes, i.e. $\boldsymbol{E}_{\mathrm{H}} = (0, 0, E_z)$ and $E_z = -\mu_{\mathrm{H}}BE_x$. A macroscopic and tangible consequence of the Hall field is the appearance of a measurable transverse voltage that is proportional to the magnetic field. This voltage is known as the Hall voltage, V_{H}, and can be calculated as:

$$V_{\mathrm{H}} = -\mu_{\mathrm{H}}BE_x w, \tag{3}$$

where w denotes the strip width. By relating the Hall mobility in Eq. (3) to the current density, it is possible to express the Hall voltage as:

$$V_{\mathrm{H}} = R_{\mathrm{H}}J_x Bw \tag{4}$$

where $R_{\mathrm{H}} = \mu_{\mathrm{H}}/\sigma = r/en$ denotes the Hall coefficient, r the Hall scattering factor of carriers and n is the carrier density, and the negative sign has been omitted. This indicates that low carrier-concentration produces a large Hall coefficient R_{H}, and explains why semiconductors are more useful here than metals are. The presence of the Hall field also results in inclination of the total electric field in the sample, with respect to the external field, by the Hall angle θ_{H} with $\tan\theta_{\mathrm{H}} = E_z/E_x = -\mu_{\mathrm{H}}B$.

Consider now the assumption of zero Hall electric field, $E_z = 0$. This condition is approximately realised by considering a short strip with wide cross-section. If an electric field $\boldsymbol{E}_{ex} = (E_x, 0, 0)$ is applied, as before, the current density given by Eq. (2) leads to another lateral component J_z, which produces a rotation of the current lines described by the ratio:

$$\frac{J_z}{J_x} = \mu_H B = \tan\theta_L \tag{5}$$

where θ_L is referred to as the carrier or Lorentz deflection angle. The longer carrier drift path brought by this deflection leads to the transversal geometric magnetoresistance effect [1]:

$$\frac{\rho_B - \rho_0}{\rho_0} = (\mu_H B)^2 \tag{6}$$

where ρ_0 denotes the electrical resistivity at $\boldsymbol{B} = 0$, and ρ_B the resistivity enhanced by the magnetic field. Eq. (6) shows that the relative change in resistivity increases with the square of the mobility-induction product. Hence this effect is very small for silicon. Sensors based on this effect require high-mobility III–V compounds such as InSb or InAs. Due to their low electron mobility, the geometrical magnetoresistivity in metals also has no practical importance.

Besides the above geometrical magnetoresistance, there is also the anisotropic magnetoresistance which is a larger physical effect occurring in ferromagnetic transition metals and alloys [4]. In these materials the magnetisation vector determines the direction along which the current normally flows. The application of an external magnetic field rotates the magnetisation vector in the sample, and thus the current path, by an angle θ. The specific resistivity of the sample as a function of θ, $\rho(\theta)$, is given by:

$$\rho(\theta) = \rho_\perp + (\rho_{||} - \rho_\perp)\cos^2\theta = \rho_\perp + \Delta\rho\cos^2\theta \tag{7}$$

where $\rho_{||}$ is the resistivity of the sample when $\theta = 0$, $\rho_\perp$ the resistivity of the sample when $\theta = 90^\circ$, θ being the angle between the internal magnetisation and the direction of the current, and the quotient $\Delta\rho/\rho_\perp$ is called the magnetoresistive effect [4]. It is common practice to consider the resistivity ratio $\Delta\rho/\rho_0$ when dealing with the magnetoresistive effect. The anisotropic magnetoresistance effect can be easily realised using thin film technology and, hence, lends itself to sensors applications.

The principle of measuring magnetic field using superconducting materials is based on the Meissner effect (the expulsion of magnetic flux) and flux quantisation which result in the constancy of the magnetic flux through a superconducting closed loop. If such a superconducting loop is placed in an external field H_{ex}, a shielding current, know as the supercurrent I_s, will circulate around the inner surface of the ring such that the total magnetic flux, Φ_i, inside the ring is quantised and composed of the flux LI_s (L is self inductance around which the supercurrent flows) and the flux Φ_{ex} of the external field:

$$LI_s + \Phi_{ex} = \Phi_i = m\Phi_0 \tag{8}$$

where $\Phi_0 = 2.07 \times 10^{-15}$ Wb is the flux quantum and m an integer. Thus the superconducting ring responds to any change in external flux by setting up an equal but opposite flux. Provided that the supercurrent value does not exceeds the critical current density, I_c, for as long as the superconducting specimen remains superconducting, Φ_i will remain constant, and quantised, at the same value. This behaviour, coupled with the Josephson effects, provides the operational basis of the SQUID [2].

Eqs. (2)–(8) represent some physical principles to develop magnetic sensors utilising dc technology. Sensors in this category include the Hall effect sensors [5,6], the magnetodiodes and magnetotransistors [7,8] which are based on the magnetoconcentration or Suhl effect [1], the GMR sensors [9], and the SQUID magnetometers [10]. The operational principles, advanced features and recent developments and applications of the SQUID magnetometer and giant magnetoresistive sensors (Eq. (7) with large resistivity ratio) are given in Sections 3 and 4.

For the case of ac technology, magnetic sensing is based on classical electrodynamics, such as Faraday's law of induction (search-coil sensors [11], fluxgate sensors [12]), and skin effect (magneto-impedance and giant magneto-impedance sensors). When ac excitation is used, the voltage V and the total current $I = I_m \exp(i\omega t)$, I_m being the amplitude, are related via the complex impedance Z:

$$V = Z(\delta)I \tag{9}$$

with δ being the skin-depth which is a function of angular frequency ω and magnetic permeability. Section 5 gives detailed description of the concepts, operational principles and technologies of GMI sensors.

2.2. Categorisation and applications of magnetic sensors

The response of a magnetic sensor is usually determined by the strength of magnetic induction $\boldsymbol{B}$ that acts on the mobile carriers. Hence, it is often boosted by employing a highly permeable material. Magnetic sensors using ferro- or ferrimagntic materials where $\mu_r \gg 1$, μ_r being the relative permeability of the sensor's material, bring about a considerable enhancement of sensitivity. Examples of such sensors are those based on magnetoresistance in NiFe thin films [13,14], or the magneto-optic effects in garnets [11]. On the other hand, all sensors based on galvanomagnetic effects in semiconductors use low-permeability materials and hence do not provide appreciable amplification [15]. A common way of comparing magnetic sensors is by the range of fields which they detect. Fig. 2 compares a number of common magnetic sensor technologies. Most of these devices are quite different from each other in construction and cost, so in making comparisons, we must take account of the application, the desired accuracy and the physical size of the sensor being used. It is also important to note that sensitivity range for each concept is often affected by the read-out electronics [11]. Regarding applications, sensors can be

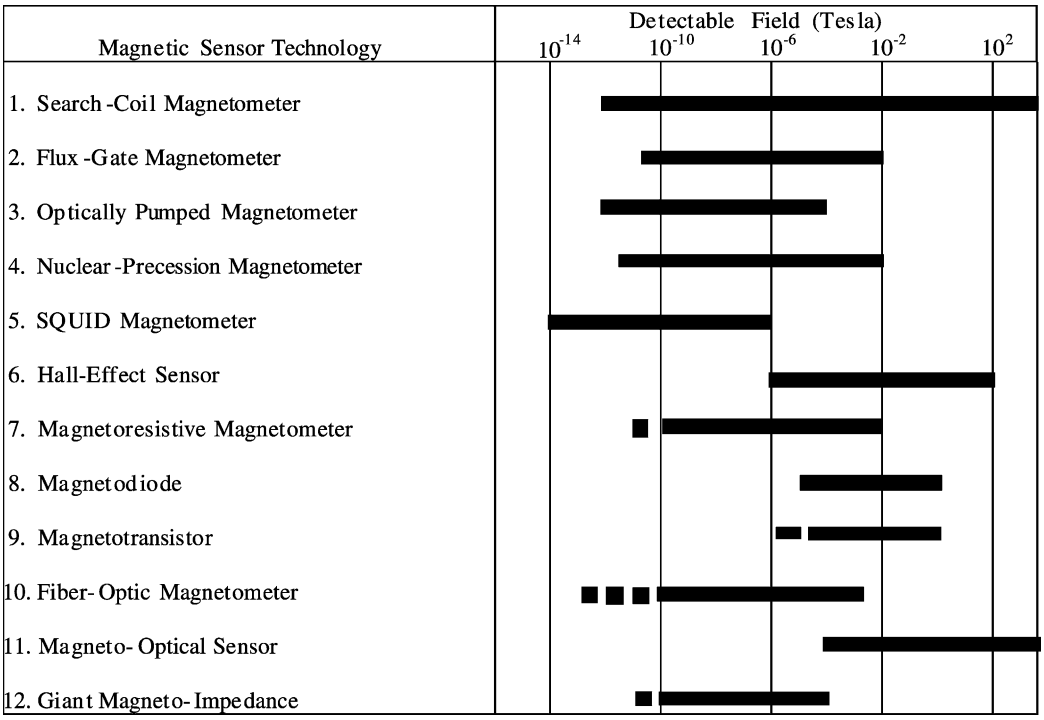

Fig. 2. A comparison list of some common magnetic sensor technologies.

Table 1
Categorisation of magnetic sensor applications

10^{-9} T		10^{-4} T
Category 3 (high sensitivity)	Category 2 (medium sensitivity)	Category 1 (low sensitivity)
Definition		
Measuring field gradients or differences due to induced (in Earth's field) or permanent dipole moments	Measuring perturbations in the magnitudes and/or direction of Earth's field due to induced or permanent dipoles	Measuring fields stronger than Earth's magnetic field
Major applications		
Brain function mapping Magnetic anomaly detection	Magnetic compass Munitions fusing Mineral prospecting	Non-contact switching Current measurement Magnetic memory read-out
Most common sensors		
SQUID gradiometer Optically-pumped magnetometer	Search-coil magnetometer Flux-gate magnetometer Magnetoresistive magnetometer	Search-coil magnetometer Hall effect sensor

classified into three basic categories as shown in Table 1 [11]. The distinction between each category is determined by how the sensor is used in relation to Earth's magnetic field [11,16]. The boundary between categories 1 and 2 results from the magnitude Earth's magnetic field, which has a strength of about 0.2×10^{-4} T. For category 1, the earth's magnetic field acts as the limiting noise source. The boundary between categories 2 and 3 is the level to which Earth's magnetic field is stable. For many applications in category 2, variations in Earth's magnetic field due to cosmological and geological effects provide the performance-limiting noise. There are many factors, such as frequency response, linearity, temperature stability, size and power, that influence what a particular sensor or sensor technology is best suited for [11].

3. SQUIDs

Since their commercialisation few decades ago, SQUIDs have evolved from a mere specialised laboratory measurement instrument that operates in the sub-nano/pico range of voltages and temperatures, to systems routinely used in such diverse applications as neuromagnetism (where signal levels of 10^{-12} T or lower are involved), magnetic resonance and geology.

Recent progress in high-T_c superconductors (HTS) technology has increased the operating temperatures of SQUID devices. On the other hand, the steady progress in HTS thin film technology has enhanced the sensitivity of these devices [17]. This has renewed various efforts to produce more commercial acceptance of these devices. In this section, the basic theory of Josephson effect and the principles of SQUID magnetometers are given. This is followed by a description of the most commonly used SQUID-based instruments and their main applications. Factors that limit the wide acceptance of SQUID-based systems are discussed in reference to recent progress in the high-temperature superconducting SQIUD technology.

3.1. SQUID magnetometer

An important application of superconductivity and Josephson junctions [18] is the magnetometer called SQUID, which has the ability to convert minute changes in current or magnetic field to a measurable voltage. This ability is based on the principles of superconductivity, the Meissner effect, flux quantisation and the Josephson effect. A Josephson junction, as named after Brian D. Josephson who discovered the structure in 1962, is effectively a weak link between two superconductors that is capable of carrying supercurrents below a critical value I_c. The 'weak link' can be either a thin layer of insulator, an area where the superconductor itself narrows to a very small cross-section, or a superconducting bridge between two superconducting sections. When a superconducting ring interrupted by a weak link is exposed to an external magnetic field, a shielding supercurrent flows around the inner surface of the ring via the weak link, as discussed in Section 2.1. However, in this case the supercurrent will be an oscillating function of the magnetic field intensity, such that it first rises to a peak as the field increases, then falls to zero then increases again and so on. In a SQUID, these periodic variations are exploited to measure the current in the superconducting ring and, hence, the applied magnetic field.

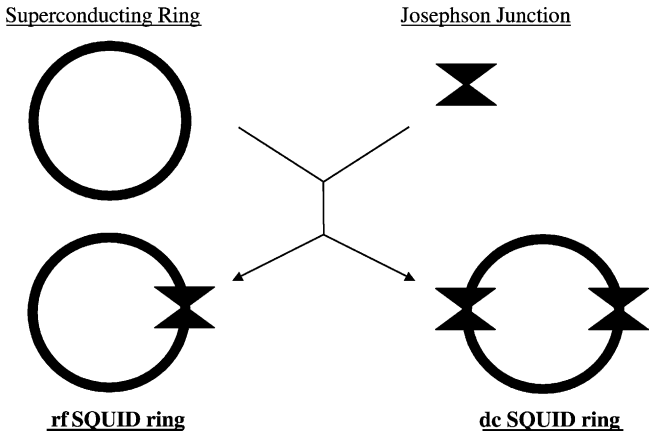

Fig. 3. Basic components of dc and rf SQUID rings.

There are two types of SQUIDs: rf and dc. In both types, the device consists of a superconducting ring interrupted by one Josephson junction, in the case of the former, or two Josephson junctions in the case of the latter, as depicted in Fig. 3. The difference between the two is in the nature of the biasing current being an rf or a dc. In either type, the special properties of the Josephson junction cause the impedance of the SQUID to be a periodic function of the magnetic flux threading the ring, so that a modulation signal applied to the bias current is used with a lock-in detector (see Fig. 4) to measure the impedance and linearise the voltage-to-flux relationship. This makes a SQUID function as a flux-to-voltage converter with highest ever known magnetic sensitivity. Also, the SQUID ring is too small to detect weak fields so a superconducting transformer with a pick-up loop forming a gradiometer, is usually added to the system. The gradiometer discriminates strongly against distant noise sources, which have small gradient, in favour of locally generated signals and thus enhance the sensitivity of the SQUID magnetometer.

Depending on the superconductors, we have low-temperature (LTS) SQUIDs operating at liquid helium temperature

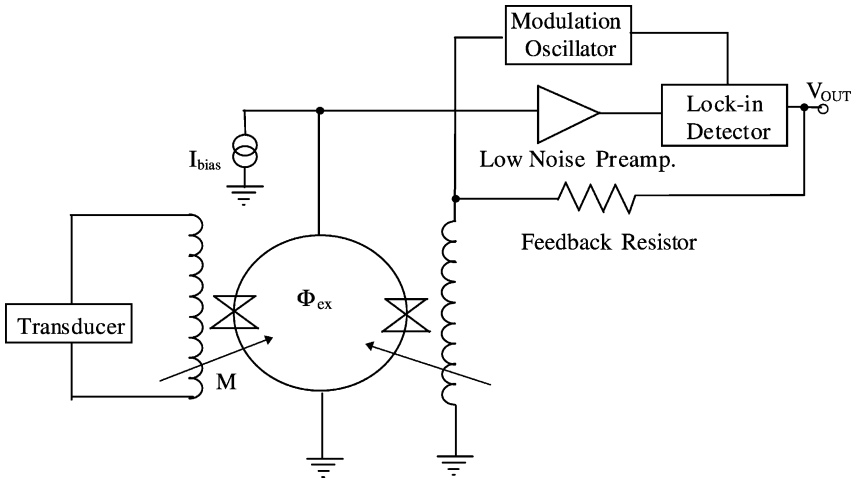

Fig. 4. A simplified circuit of a flux-locked dc SQUID magnetometer.

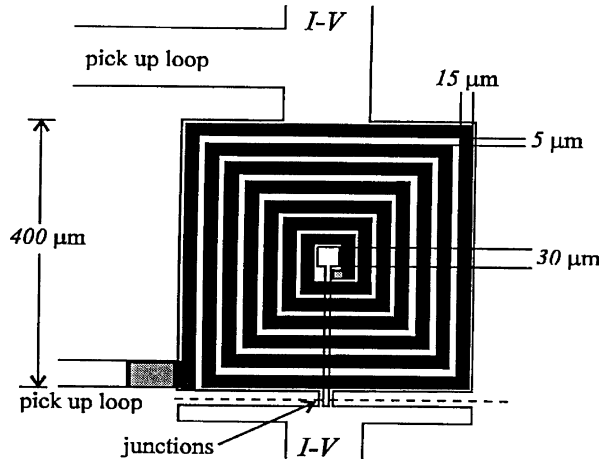

Fig. 5. A schematic diagram of a washer-type HTS dc SQUID.

(4.2 K), and high-temperature (HTS) SQUIDs operating at liquid nitrogen temperatures (77 K and above) [18]. LTS devices are mostly dc SQUIDs, while HTS devices can be either dc or rf SQUIDs, fabricated from the ceramic oxide known as YBCO. A schematic representation of typical washer-type, transformer-coupled dc HTS SQUID is shown in Fig. 5 [19]. In terms of performance, SQUIDs have excellent characteristics that comprise true dc response, wide band-width, zero phase distortion and, for the LTS type, energy sensitivity better than 10^{-32} J/Hz (equivalent to a magnetic flux noise of $10^{-6}\Phi_0\,\mathrm{Hz}^{-1/2}$ at frequencies down to few Hz), as well as high degree of linearity and dynamic range. However, a complete SQUID magnetometer comprises extra coupling and read-out units to the basic SQUID ring, as shown in Fig. 4. Hence, although a flux sensitivity equivalent to a fraction of a flux quantum, Φ_0, is theoretically possible, the actual sensitivity of a SQUID magnetometer is dependent on the sensitivity of the added units and on the intrinsic and external noise [18]. Different noise cancellation methods using gradiometers of various orientations and orders, with additional filtering techniques, have been developed and successfully used to improve the sensitivity of SQUID magnetometers particularly in cases where weak magnetic signals immersed in noise are to be detected in unshielded environments [20].

3.2. SQUID-based instruments and applications

A SQUID can be configured to measure any electromagnetic quantity. Table 2 (adopted from [21]) show the measurement capabilities and basic configurations of SQUID-based instruments. Both dc and rf SQUIDs have been used as sensors in a far-ranging assortment of instruments for a variety of applications particularly in biomagnetism and non-destructive evaluation.

Biomagnetism is broadly defined as the development and non-destructive application of magnetic field measurements on people in order to detect, locate and diagnose defects and other imperfections. The order of magnitude of the human magnetic fields ranges from about 1 nT down to less than 1 pT, as indicated in Fig. 6 [18]. Until the development of SQUIDs, the detection of magnetic fields arising from biological functions was almost unknown. LTS SQUIDs were first used in biomagnetism in 1970s, when Cohen et al. [22] recorded the magnetocardiogram (MCG), and then the magnetoencephalogram (MEG) [23]. In the mid-1980s, the improved LTS technology using niobium/aluminium-oxide/niobium Josephson junctions, with improved read-out electronics, helped the growth of multi-channel systems for both heart and brain measurements. Since then, SQUIDs magnetometers have been extensively used in a number of medical research and biomagnetism applications, as shown in Table 3. There are now systems with more than 30 LTS SQUID sensors for MCG measurements and over 100 sensors for MEG measurements [24].

Immediately following the discovery of HTS materials, HTS SQUID magnetometers which operate at 77 K were developed [25]. Later developments in HTS and thin film technology considerably improved SQUID magnetometers sensitivity and made it entirely adequate for geographical and magnetocardiology applications [24]. A nine-channel HTS SQUID MCG system has been developed and tested in an unshielded environment, and a noise level of 1 pT/Hz$^{1/2}$ for each channel has been measured [26]. Most recently, an eight-channel HTS SQUID MCG system with encapsulated

Table 2
Measurement capabilities of a SQUID-based instrument

Measurement	Sensitivity
(a) Current (A/Hz$^{1/2}$)	10^{-12}
(b) dc voltage (V)	10^{-14}
(c) dc resistance (Ω)	10^{-12}
(d) Mutual/self inductance (H)	10^{-12}
(e) Magnetic moment (emu)	10^{-10}
(f) Magnetic fields (T/Hz$^{1/2}$)	10^{-15}

Table 3
Current applications of SQUID magnetometers in the medical field

Studies of the brain—neuromagnetism
Epilepsy
Presurgical cortical function mapping
Drug development and testing
Stroke
Alzheimer's
Neuromuscular disorders
Prenatal brain disorders
Studies of the heart—magnetocardiography
Arrhythmia
Heart muscle damage
Fetal cardiography
Other medical applications
Studies of the stomach—gastroenterology
Intestinal ischemia
Non-invasive in vivo magnetic liver biopsies
Lung function and clearance studies
Nerve damage

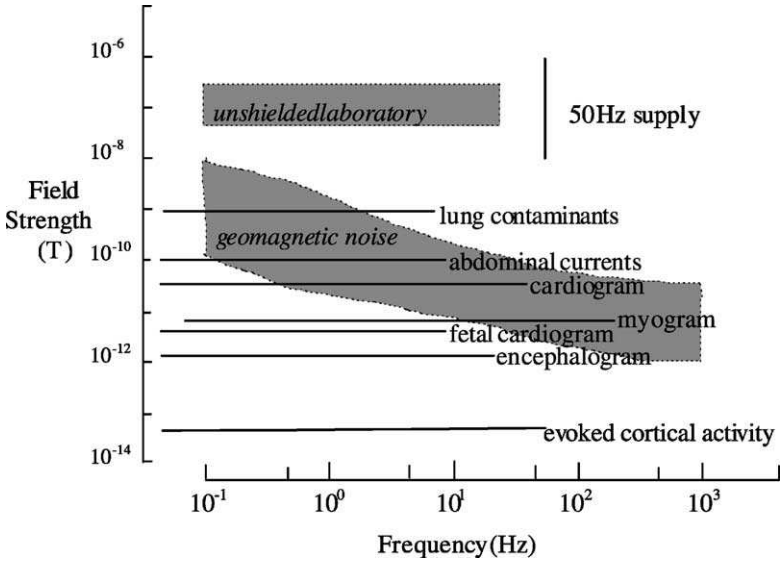

Fig. 6. Typical amplitudes and frequencies of biomagnetic signals and common noise sources.

sensors and first-order gradiometers achieving a typical noise of less than 50 fT/Hz$^{1/2}$ in a magnetically shielded chamber have been reported [27].

The excellent performance characteristics of SQUIDs afford them a deeper look into metallic structures, and permit a wide range of non-destructive testing techniques, such as imaging and hysteretic magnetisation. Both LTS and HTS SQUIDs have been used for applications such as, for example, inspection of cladded pipes, airplane wings, corrosion pits and stress fracture [21]. LTS and HTS scanning microscopes have also been demonstrated. For example, a niobium SQUID loop 4 μm in diameter and 0.8 μm line width has been used to map flux quanta penetration in and around a Josephson logic circuit [28]. On the other hand, a resolution of 130 μm has been achieved in the measurement of a feature of a dollar bill using a HTS SQUID loop of 140 μm [28].

3.3. High-T_c SQUIDs magnetometer and future needs

The convenience of operating in the 40–80 K temperature range has opened up new possibilities of SQUID applications, most of which require high sensitivity and mechanical ruggedness in their operating conditions.

Over the past few years, YBCO films quality and crossover design techniques have improved, thus reducing the flux-motion noise by eight orders of magnitude since the earliest HTS production. This has been achieved via (both) different fabrication techniques of junctions, such as the YBCO boundaries microbridges and nanobridges, single and multilayers, different seed layer materials [29], and the application of various active noise compensation techniques [30]. HTS SQUIDs with noise figures of 9.7 fT/Hz$^{1/2}$ at 1 kHz and 53 fT/Hz$^{1/2}$ at 1 Hz have been reported [17]. Fairly recently, planar dc SQUID gradiometers based on YBCO thin films with a gradient resolution of 450 fT/(cm Hz$^{1/2}$), were prepared and tested in unshielded environment [31]. Based on these gradiometers, a biomagnetic two-channel system which operates directly in the hospital for investigation of cardiac infraction has been developed [31].

Although this is still way behind the sensitivity performance of the state-of-the-art LTS SQUIDs, it seems possible that by improving the fabrication process and material properties, more robust HTS SQUIDs can be obtained. This, for example, could be achieved by adopting a combination of configurations, together with additional active noise compensation techniques. On the other hand, advanced read-out and interface electronics with fast slew-rates [32] will be beneficial for all SQUID-based applications. In fact, this coupled with state-of-the-art signal processing that offers real-time signal averaging, visualisation and storage option, may prove of a significant value to physicians, for example, in the case of SQUID-based biomagnetism systems.

Another aspect lies in providing appropriate cooling systems for SQUIDs that are easier to take care of compared to the liquid cryogen filled dewars. This could reduce the delicacy of SQUID-based instrument and make them user-friendlier. In fact, this has been one of the major challenges for workers in the field over the last two decades. A significant progress in the development of various cooling systems for HTS SQUIDs, such as pulse tube refrigerators (PTR), have been achieved. Recently, a HTS SQUID-based sensor cryocooled by liquid nitrogen has been developed for the detection and classification of underwater magnetic targets such as sea mines and unexploded ordnance [33].

Ideally, the best solution towards more acceptable SQUID-based systems is to make them more closely resemble a ‘black box’ with a user-friendly monitor, such that users do not even recognise the SQUID or feel any of the cryogenics aspects involved.

4. Giant magneto-resistance (GMR)

This technology has evolved recently from the rather better known anisotropic magnetoresistance (MR) sensing technology that came about since a landmark paper by Hunt [34]. Even MR technology is still new and continues to develop with advances in materials and electronic circuits which take it to new levels. Therefore, it is necessary to describe MR technology first in order to appreciate GMR technology and to realise the latest capability of MR itself.

4.1. MR sensors

The magnetoresistance phenomenon in which the electrical resistance of a conductor made from a magnetic material changes in the presence of a magnetic field, as described in Section 2.1, has been known for more than 100 years. It has only become important as a magnetic sensor since R.P. Hunt reported that, when a permalloy thin film is made, its electrical resistance can change by up to about 2% when its magnetisation direction is changed (by an external field) from a direction parallel to the current flow by an angle of 90° to the current flow. More importantly, when the film is made (photolithographically) into a small size and magnetisation is set in a "single domain" state then the noise in the sensor is vanishingly small and almost only limited by the Johnson noise so that a signal-to-noise ratio of up to 97 dB can be achieved. In an application in magnetic recording there was about 20 dB of "tape" noise so even taking account of this, MR technology was still much better than its inductive counterpart, especially as, for modern magnetic recording and data storage systems, very small data tracks are used with a requirement for small replay transducers with very small electrical signals requiring good signal-to-noise ratio. MR technology has consequently been driven hard by data storage but, in parallel with this it has found increasing applications in magnetic sensing, particularly in areas where very small size has not been a requirement [35].

MR sensors are commonly made from ferromagnetic thin films. This has two major advantages over bulk materials: the resistance is high and the anisotropy can be made uniaxial [36]. The ferromagnetic layer behaves like a single domain and has one distinguished direction of magnetisation in its plane called the easy axis, which is the direction of magnetisation without external field influence. The basic thin film MR is an evaporated thin layer of suitable material such as 80/20 nickel–iron on a non-magnetic flat substrate. The electrical resistance of the film can be modulated by the application of a magnetic field which changes the direction of its inherent magnetisation. Such a film can have a typical size of, say 50 mm × 10 mm × 20 nm. The small thickness is a result of recent advances—even thicknesses much smaller than this are now viable. For the latest computer disk drive heads, the height and width of the sensor is much reduced to only a few microns. In this case, an optimum performance is achieved by a bias system based on compiling to a soft adjacent layer (SAL). This IBM-developed biased MR structure, shown in Fig. 7, is widely used in IBM's MR suspended head design which consists of separate read and write elements sharing a common layers [37].

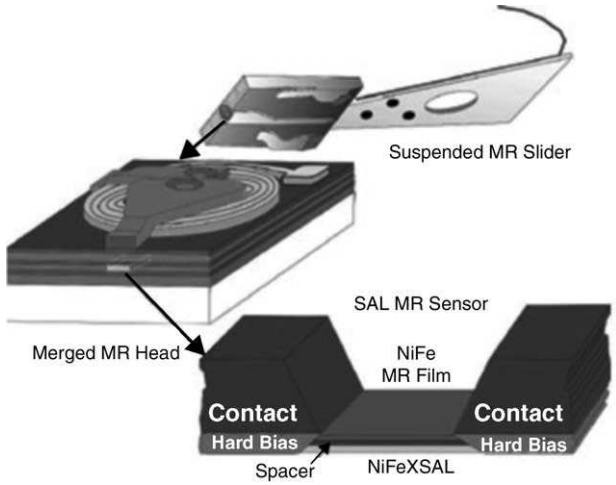

Fig. 7. A SAL MR sensor as used in the basic IBM suspended head design (courtesy of IBM storage systems division, IBM—see [37]).

4.2. Linearity of MR sensors

The fundamental characteristic of magnetoresistors, particularly the anisotropic type, is not only non-linear but it is subject to hysteresis. A summary of the limitations of magnetoresistance in terms of linearity can be found in [38]. The non-linearity relates mainly to the cosine-squared relationship between the magnetoresistance and the angle θ of the magnetisation, as indicated by Eq. (7) (also, see [35]). In practice, this is modified by saturation effects so that there is a point of inflection on the curve where there is a sensibly linear range. If the sensor is biased at this point a good linear response can be achieved. Different biasing methods are used in order to linearise the operation of MR sensors. One of those is the 'barber-pole' configuration [39], where narrow gold strips are deposited in an oblique direction with respect to the length of the sensing element. The magnetic field response becomes linear and passes through the origin for a zero dc applied field. Wheastone half- and full-bridge configurations are used by companies like Philips (KMZ51, KMZ10A MR sensors), Honeywell (HMC1001) or San Diego Magnetics (SDM531). The first three devices have no flux concentrators and their white level is in the range of 50–100 $pT/Hz^{1/2}$ [40].

A biasing technique, commonly used in MR head design, is that based on the IBM-developed SAL biased MR structure. As indicated in Section 4.1, this structure consists of the MR NiFe film as well as a magnetically soft alloy layer separated by a film with high electrical resistance (see Fig. 7). A bias current continuously passes through the MR sensor, monitoring its resistance. A non-linear resistance change oc-

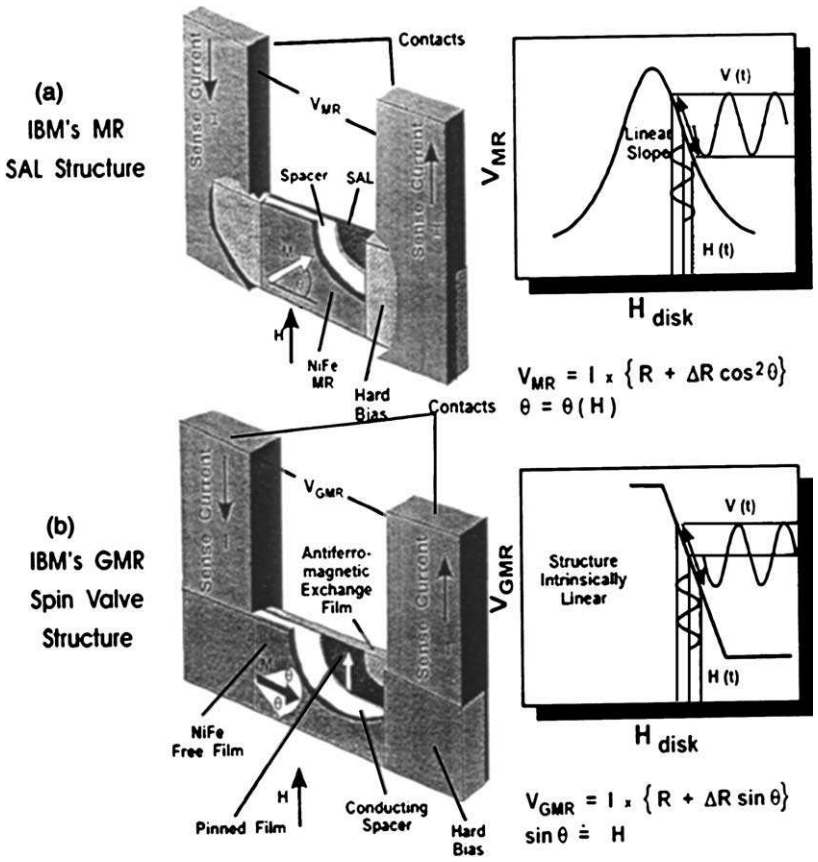

Fig. 8. The general structure of the IBM SAL biased MR and GMR spin-valve sensor for magnetic recording.

curs as this sensor passes through the disk's magnetic field. The bias current also creates a magnetic field that interacts with the magnetisation of the underlying soft film, saturating it. This transverse biasing results in magnetic rotation in the MR film at an angle to the bias current, producing linearisation of the MR signal, as shown in Fig. 8(a) with a resistance change up to 0.8%/Oe in some cases. To maintain stability and suppress magnetic domain noise, a longitudinal bias is applied by an additional structure referred to as the hard bias layer. This is configured at the contacts adjacent to the MR element in a patterned configuration, as shown in Fig. 7.

A recent advance is to apply a switched-bias to a pair of such sensors [41,42]. In this system, each sensor is placed in a square-wave transverse field which switches the bias from one side to the other of the MR characteristic loop. The outputs from the two sensors are subtracted in a differential amplifier to produce a zero output except if the system is unbalanced. The field to be detected unbalances the system, producing a non-zero square-wave output proportional to the magnitude of the field. When combined with a lock-in amplifier, this system is extraordinarily sensitive and can reach the nano-Telsa range of detection. A curve from [42] is reproduced as Fig. 9 showing an excellent output level for an applied field of 160 nT. The best output level of 24 mV from this system is accompanied by a noise level of less than 1 mV. The switched-bias technique is still in its infancy and, so, represents a new horizon for these sensors, much of which remains to be realised.

4.3. GMR sensors

The phenomenon of giant magnetoresistance (GMR) was first reported by Baibich et al. [43]. The original discovery concerned a series of multi thin film layers of iron and chromium which produced changes in electrical resistance of greater than 50% at low-temperature (~4 K) when subjected to large fields of thousands of Oersteds. Rapid development of devices using this effect resulted because of a need for better reproducing heads in magnetic recording at room temperatures and detecting small fields. Nowadays sensors are of micron dimensions and can produce >10%/Oe resistance change at room temperatures [44]. The basic system now is the so-called "spin-valve" which achieves large change in resistance at or near the zero field axis (Fig. 10). A typical configuration is shown in Fig. 8(b) (taken from [45]).

The spin-valve differs from the original GMR system in some important respects. The system of Baibich et al. was a repetitive Fe/Cr multilayer with a large number of alternate layers. When all these layers were magnetised the same way, half of the spin-polarised conduction current electrons could move through the sandwich with no appreciable scattering in the magnetic material (low resistance) whereas when the

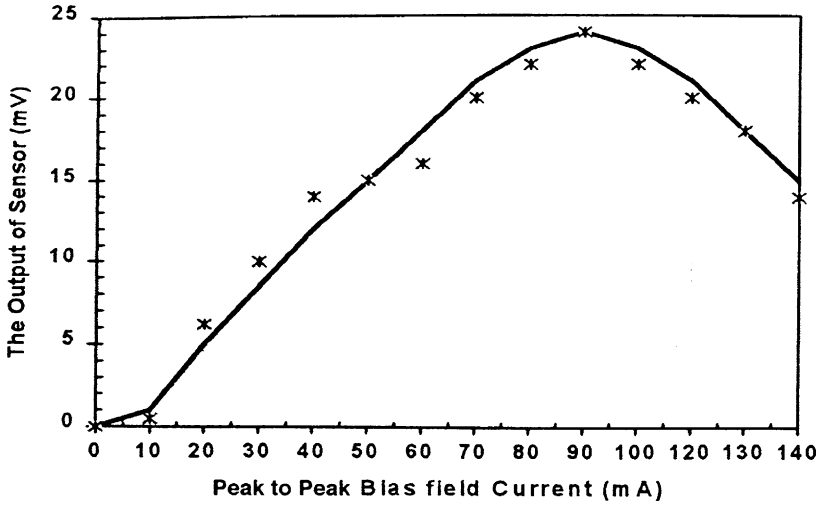

Fig. 9. The output of 10 nm sensor vs. 250 Hz bias field (0.009 Oe/mA) for an applied field (δH) of 160 nT.

magnetisation in alternate layers is reversed there is always some scattering for all the electrons no matter whether they are "spin up" or "spin down". The spin-valve is much simpler with only (basically) four layers. An antiferromagnetic exchange film (e.g. Mn, Fe) couples to a cobalt layer and pins its magnetisation in a (say) transverse direction. A second magnetic film is separated from the soft NiFe layer by a very thin conducting layer (Cu). This magnetic film has a variable magnetic direction determined by the field to be sensed and as the magnetisation angle between the two magnetic films changes, so the scattering of electrons moving through the combined structure is varied. This gives a resistance variation which is much larger than for simple MR.

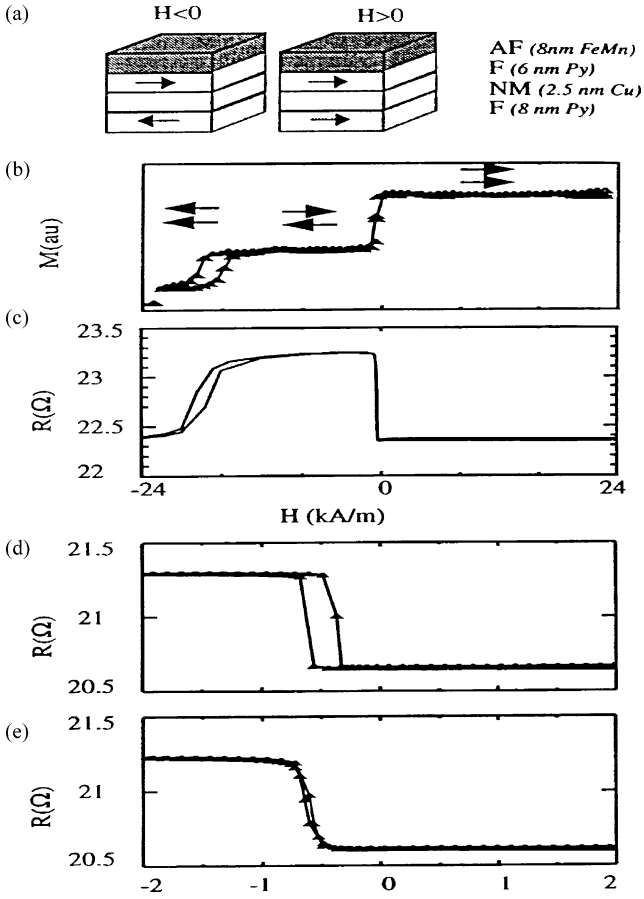

Fig. 10. (a) Schematic configuration of a spin-valve (basic layout); (b) measured magnetisation curve of a spin-valve; (c) measured magnetoresistance curve of a spin-valve; (d) low field MR response for parallel easy axes; and (e) low field MR response for crossed easy axes.

Regarding sensitivity, GMR and spin-valve devices with field noise power of about 20 pT/Hz$^{1/2}$ at 100 Hz and a calculated Johnson noise limit of less than 6 pT/Hz$^{1/2}$ above 1 kHz have been recently reported [40]. Interesting data may also be found in [46], which addresses the $1/f$ noise in GMR and spin-valve reading heads.

4.4. Spin tunnelling

Another effect of some significance is found by making the layer in the centre of the magnetic "sandwich" from a very thin insulator instead of a conductor—the so-called tunnelling effect [47] spin-polarised electrons passing through the thin insulator from one magnetic layer to the next are susceptible to the relative magnetic directions on either side of the barrier giving a magnetically-dependant effect on the contact resistance. This so-called tunnel junction is very difficult to control so that a reasonably low resistance is achieved for, say, an oxidised alumina barrier layer. Control of the oxidation of the interface is important [48] but MR ratio can be as high (e.g. 23%) as for more well-known GMR devices.

5. Giant magneto-impedance (GMI)

The giant magneto-impedance (GMI) effect includes a large and sensitive change in an ac voltage measured across

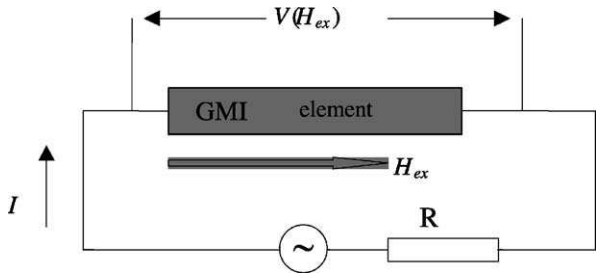

Fig. 11. Simplified circuit for GMI.

a soft magnetic specimen subjected to a high frequency current under the effect of a dc (or lower frequency) magnetic field. A typical circuit is shown in Fig. 11. Two conditions are important to get a large change in impedance: (i) the frequency of the excitation current must be such to insure a strong skin effect, and (ii) the magnetic structure has to provide an ac transverse permeability sensitive to the external field. At frequency of few MHz, these conditions are realised in 30 μm diameter CoFeSiB amorphous wires having circular domain structure, showing the impedance change as much as 40–100%/Oe [49,50]. Because of its high sensitivity in combination with other advantageous properties, the GMI effect has received much attention as a candidate to develop new generation micro-magnetic sensors. Magnetic sensors based on GMI in amorphous wires have been recently developed, which demonstrate the field detection resolution of 10^{-6} Oe for the full scale of ±1.5–2 Oe with a sensor head length of less than 1 mm, and power consumption of less than 10 mW [51].

GMI can be considered as a high frequency analogy of giant magnetoresistance. In the latter case, the sensitivity to the field is relatively low and does not exceed 1.5%, as was discussed in Section 4. Besides, there are hysteresis and temperature instability problems. GMI elements typically exhibit no hysteresis for the variation in the applied field. Compared with a flux gate element, which also has a very high sensitivity, the GMI element can be 100 times smaller and its response speed up to 10 MHz is more than 10^3 times higher. In terms of sensitivity, GMI cannot still reach the lower level of that for SQUID magnetometer, however, the GMI element seems can satisfy all the general requisite conditions for various field and current sensors.

5.1. GMI effect

The complex impedance Z that determines the measured voltage at an ac excitation (see Eq. (9)) is a function of the skin penetration depth. In the case of a magnetic wire with radius a, length l, resistivity ρ and circumferential permeability μ_φ, the impedance Z is generally expressed by an equation involving the Bessel functions as shown by Eq. (10) of Table 4. The magnitude of Z is sensitively changed by an external field H_{ex} due to the relation of $Z \propto \sqrt{[\omega\mu_\varphi(H_{ex})]}$ at the condition of a strong skin effect ($\delta \ll a$). The skin effect occurs at frequencies over 130 kHz in an amorphous wire having ρ of 130 μΩ cm, a of 15 μm, and a dc maximum differential permeability (relative permeability) of 10^4 measured by the circumferential dc BH hysteresis loop.

For the case of a wire having a circular domain structure, the symmetrical impedance changing characteristics as the skin effect gets stronger are analysed as follows. The magnitude of the wire impedance $|Z|$ monotonically decreases with increasing H_{ex} for angular frequencies of $1 < \omega/\omega_{\delta 0} < 20$, where $\omega_{\delta 0} = 2\rho/a^2\mu_{d0}$ is a characteristic frequency at which the skin-depth equals to the wire radius for the case of a constant permeability μ_{d0}. In this frequency region, the domain-wall movement contributes dominantly to μ_φ. For higher frequencies $\omega > 30\omega_{\delta 0}$, $|Z|$ increases with H_{ex} until H_{ex}/H_K (H_K is the anisotropy field) and then decreases with increasing H_{ex} ($>H_K$). This behaviour is related to the rotational mechanism for μ_φ since the domain-wall movement is strongly suppressed by a large eddy current damping effect. It has been found that an optimal bias field H_b of about half value of H_K and an optimal angular frequency ω^* of (200–600)$\omega_{\delta 0}$ are required to realise the most field-sensitive sensor head using the amorphous wire. The values of the optimal magnetisation frequency f^* are 30–120 MHz for the amorphous wire with $a = 15$ μm, $\rho = 130$ μΩ cm, and $\mu_{d0} = 10^4\mu_0$.

5.2. GMI in Co-based wires

One of the best materials for GMI is a $(Co_{1-x}Fe_x)_{72.5}Si_{12.5}B_{15}$ amorphous wire which has a negative magnetostriction for $x < 0.06$. In the outer layer of the wire, the compressive stress from quenching coupled with the negative

Table 4
Expressions for impedance in a wire

Expressions for impedance	Comments	Equation number
$Z = R_{dc}ka(J_{b0}(ka)/2J_{b1}(ka));$ $k = (1-i)/\delta,\ \delta = \sqrt{(2\rho/\omega\mu_\varphi)},\ \mu_\varphi = \mu'_\varphi - i\mu''_\varphi$	Valid for any frequency, μ_φ is the linearized circumferential permeability averaged over domains, R_{dc} the dc resistance, a the radius, l the length, ρ the resistivity and J_{b0}, J_{b1} are Bessel functions	(10)
$Z = R_{dc} + i\omega L_j,\ L_j = l\mu_\varphi/8\pi$	Low frequency expansion (weak skin effect: $a \ll \delta$)	(11)
$Z = R_{dc}(a/2\sqrt{2\rho})(\sqrt{\mu_R} + i\sqrt{\mu_L})\sqrt{\omega};$ $\mu_R = \lvert\mu_\varphi\rvert + \mu''_\varphi,\quad \mu_L = \lvert\mu_\varphi\rvert - \mu''_\varphi$	High frequency expansion (strong skin effect: $a \gg \delta$)	(12)
$\lvert Z\rvert = \sqrt{R_{dc}l/4\pi}\sqrt{\omega\lvert\mu_\varphi\rvert}$	Absolute value of impedance for a strong skin effect case ($a \gg \delta$)	(13)

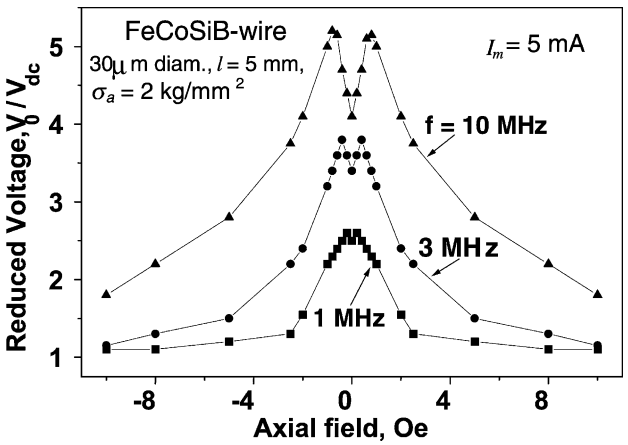

Fig. 12. Normalised voltage amplitude V_0/V_{dc} vs. axial field for different frequencies in a FeCoSiB amorphous wire subjected to the ac sinusoidal current of amplitude $I_m = 5\,mA$. V_{dc} is the dc voltage level. The wire is annealed under a tensile stress of $\sigma_a = 2\,kg/mm^2$, it has a diameter of 30 μm and a length $l = 1\,mm$.

magnetostriction results in the circumferential anisotropy and an alternate left and right handed circular domain structure [52]. This structure is retained even for wires with slightly negative magnetostriction of -10^{-7} ($x = 0.06$), for which especially large and sensitive GMI effects have been reported. Annealing under tensile stress enhances the circumferential anisotropy, and the circular domain structure exists almost in the entire wire.

The GMI characteristics for a sinusoidal current magnetisation are represented in Fig. 12. The magnitude of the voltage monotonically decreases with increasing H_{ex} for the magnetising frequency $f = 1\,MHz$. In the case of a higher frequency $f = 10\,MHz$, it increases for $H_{ex} < H_K$ and then decreases with $H_{ex} < H_K$. The high frequency behaviour of the impedance is in line with that for rotational permeability. The impedance changing ratio increases if the sinusoidal current is biased with a dc current which makes a single domain at the surface layer of the wire, reaching a value of more than 100%/Oe, which is typically more than 10 times higher than that of the GMR element.

5.3. Asymmetrical GMI

The fundamental GMI characteristics are not only non-linear, but also shaped in a way that the operation near the zero-field point can present serious problems. Generally, a dc bias field is used to set properly the operating point on the GMI characteristics. If then two oppositely biased elements are connected in a differential structure, a near-linear output occurs in some field interval near the zero point. However, applying the dc bias field increases substantially electric power consumption. In some cases, the use of additional coils to produce the bias field may be non-desirable as well. The effect of the bias field can be regarded as producing asymmetry with respect to the sensed field, H_{ex}. Therefore, for linear sensing the asymmetrical GMI (AGMI) is of great importance.

AGMI characteristics at a frequency of 1 MHz have been reported [53,54] for the case of a twisted amorphous wire having a helically-induced magnetic anisotropy, subjected to an ac current, $I = I_m \sin \omega t$, biased with a dc component I_b. Without a dc bias current I_b, there are two symmetrical picks. Applying I_b produces asymmetry in GMI behaviour and increases the sensitivity. In the case of $I_m = 7.5\,mA$ and $I_b = 4\,mA$ one of the original picks is almost suppressed, whereas the sensitivity of the other becomes as high as 120%/Oe. However, a stress relaxation would occur in the wire twisted and fixed at its both ends with soldering, which gradually changes the sensor characteristics. Stable AGMI characteristics can be obtained if the helical anisotropy is induced by annealing under twist. In this case, asymmetry becomes more pronounced with increasing the dc bias and the sensitivity increases up to about 100%/Oe for $I_m = 14\,mA$ and $I_b = 7.5\,mA$. If then two oppositely biased AGMI elements are connected together in the differential system, a near voltage response appears in the field interval of ±2 Oe with the voltage change of ±80 V.

Another method to produce asymmetry is related to utilising an ac bias field h_b [55]. In this case, the helically-induced anisotropy is not required, and an asymmetrical voltage response can be obtained in a wire with a circumferential anisotropy. The ac bias is generated by an ac current in the external coil, which can be the same as the current I flowing in the GMI element. This auto-biased configuration has been realised in a wire with a circumferential anisotropy, driven by a pulse current I_P (having both low and high frequency harmonics) flowing through the wire and the coil mounted on it, as shown in Fig. 13.

5.4. GMI in films

Compared to CoFeSiB amorphous wires, sputtered Co-rich amorphous films typically exhibit a lower GMI sensitivity of 4–10%/Oe because of a higher anisotropy field induced during the fabrication process and annealing [56]. A very sensitive GMI has been recently reported to occur in magnetic/metallic multilayers, in which the impedance change ratio is several times larger, then that in a similar ferromagnetic single-layer film. For example, in CoFeSiB/Cu/CoFeSiB films of 7 μm thick the GMI ratio is

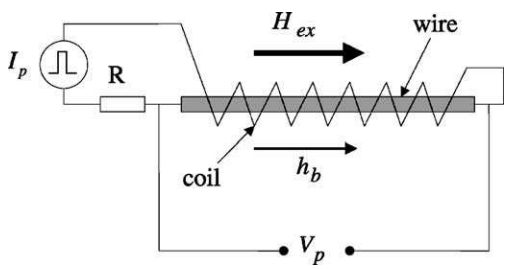

Fig. 13. Principle electronic circuit for ac (pulse) biased AGMI.

340% for a frequency of 10 MHz and a dc magnetic field of 9 Oe. On the other hand, in the CoFeSiB layer of the same thickness, the impedance varies over few percents under these conditions [57].

A typical multilayer structure for GMI comprises two outer magnetic layers with transverse magnetic structure and an inner conductive lead having a much higher conductivity (the conductivity ratio for the amorphous/Cu multilayers is about 50). In this case, a very large change in impedance can occur at much lower frequencies when the inductance related to the outer magnetic layers becomes larger than the resistance determined mainly by the inner conductor. Under the condition of a week skin effect, the impedance is given by [58]:

$$Z = R_{\mathrm{m}}\left(1 - 2j\mu_{\mathrm{t}}\frac{d_2 d_1}{\delta_1^2}\right) \tag{14}$$

where R_{m} is the resistance of the conductive lead, μ_{t} the averaged transverse permeability, $2d_1$, d_2 the thickness of the conductive and magnetic layers, respectively, δ_1 is the skin-depth in the inner conductor. Eq. (14) can be compared with GMI in a single magnetic layer in which a large magnetic response of Z is possible only in the case of a strong skin effect, when $Z \propto 1/\delta_2 \propto \sqrt{\omega\mu_{\mathrm{t}}}$. On the other hand, the GMI effect in a sandwich film can be very large even at relatively low frequencies when the skin effect is not essential, having a linear dependence on μ_{t}. For a frequency of 10 MHz, taking $d_1 = d_2 = 0.5\,\mu\mathrm{m}$ and $\sigma_1 = 2.2 \times 10^8$ S/m (conductivity of Cu), the parameter $d_1/\delta_1 = d_2/\delta_1 = 0.045$. A typical low frequency change in μ_{t} (having a rotational mechanism) under the application of $H_{\mathrm{ex}} \cong H_{\mathrm{K}} = 10\,\mathrm{Oe}$ is from 1 to 10^3. This change corresponds to over 400% variation in the impedance, which explains the experimental results. Due to this advantage, GMI in sandwich films has a potential in developing sensitive micro magnetic sensors and magnetic heads for high-density magnetic recording.

5.5. GMI applications and circuitry

Using GMI elements, new sensitive and quick response micro magnetic sensors are being developed for advanced intelligent measurement and control system [51], including non-destructive testing, highly accurate rotary encoder heads, medical electronics, and automobile control. In this section, the basic principles of GMI sensor operation are discussed.

To realise high frequency operation and avoid microwave problems, such as impedance mismatching, the GMI elements have to be assessed for use with self-oscillation circuits, such as Collpits oscillator (see Fig. 14) or multivibrator. To obtain good linearity and stability, the GMI circuits have to be completed with a detector (de-modulator), a differential amplifier and a negative feedback loop. Typical sensor characteristics with Colpitts oscillator having a frequency of 50–100 MHz are: field sensing resolution is 1 μG for ac fields and 10 μG for dc fields; quick response operation up to 1 MHz; and non-linearity is less than 0.2% FS (±1 Oe). This means that the spectral white noise density is of the order of 100 fT/Hz$^{1/2}$. To construct a linear field sensor (with AGMI) or a gradient-field sensor, a pair of GMI elements can be used in multivibrator circuit. The gradient-field sensor is suitable to detect small localised fields as a magnetic-pole field (cancelling a uniform disturbance field such as a terrestrial field). For example, a pin-hole as small as 100-micron diameter in a steel sheet of 0.2 mm thick running with a speed of 10 m/s can be detected with this sensor at a gap of 5 mm [51].

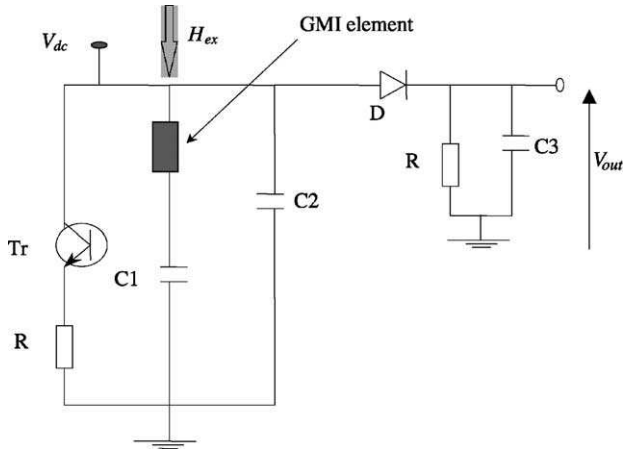

Fig. 14. Colpitts oscillation circuit for MI sensor. The circuit operates from dc voltage source V_{dc}, axial sensed magnetic field H_{ex} is applied to the MI element, V_{out} is the circuit output which is a function of H_{ex}.

A more advanced circuit to explore GMI characteristics is C-MOS IC multivibrator reported by Kanno et al. [59]. This circuit produces sharp-pulsed current of duration 2–10 ns. Such pulsed current involves both high frequency (100–500 MHz) and low (quasi-dc) harmonics. Therefore, it can be ideally used for the asymmetrical response requiring dc or ac bias. This circuit also has a good stability since C-MOS multivibrator oscillation frequency almost does not depend on the impedance characteristics of the GMI films. Power consumption of this circuit is also small (10 mW).

6. Conclusions

SQUID magnetometers are, undoubtedly, the most sensitive of all magnetic sensors and outperform conventional electrical and magnetic sensing techniques in many areas. However, despite all the progress in the technology over the past few decades, the commercial success of SQUID-based applications is still limited. This has mainly been due to the inevitable high system price which in most cases overrides the advantages of these systems in comparison with other competing methods. The discovery of HTS materials and recent advances in the SQUID and thin film technology,

have again open the possibilities for broader acceptance of SQUID-based applications. The current state-of-the-art HTS SQUID technology is still lagging behind their LTS counterparts in terms of sensitivity. However, driven by continuous advances in thin film and microelectronics technologies, progress in fabrication techniques of HTS SQUIDs is encouraging. This is coupled with improvement in read-out/interfacing electronics, and the development of alternative and easy to use cooling systems, offer potential for the development of more convincing SQUID systems with more extended applications, some of which have been briefly discussed here.

Despite their relatively recent introduction to the field, GMR and GMI materials have already started to expand the horizons of magnetic sensing. The technologies behind these devices, particularly the thin film for GMR and the multilayer structures for GMI, easily lend themselves to very small components with high-speed capabilities. In the case of the GMR devices, an added advantage is their very simple, well-balanced operating scheme that is based on Wheastone bridge configurations. Integration of such devices with conventional semiconductor technology is hence easy, and promises significant developments in the field of advanced intelligent sensor systems. The technology can also be extended to other smart measurement and control systems. However, most existing GMR and GMI devices exhibit a rather large $1/f$ noise and Barkhausen noise due to magnetic domain trapping and motion inside flux-guides, which could severely limit their applications. Practically, we should not forget that most of these devices are still under development and, hence, with better materials quality, use of monodomain structures and advanced magnetic biasing strategies the situation could dramatically change.

References

[1] H. Baltes, R. Castagnetti, Magnetic sensors, in: S.M. Sze (Ed.), Semiconductor Sensors, Wiley, New York, USA, 1994, Chapter 5, pp. 205–270.

[2] H. Koch, SQUID sensors, in: K. Boll, K.J. Overshoot (Eds.), Sensors: A Comprehensive Survey: Magnetic Sensors, vol. 5, VCH Verlagssgesellschaft, Weinhiem, 1989, Chapter 10, pp. 381–423.

[3] R. Popovi, W. Heidenreich, Magnetogalvanic sensors, in: K. Boll, K.J. Overshoot (Eds.), Sensors: A Comprehensive Survey: Magnetic Sensors, vol. 5, VCH Verlagssgesellschaft, Weinhiem, 1989, Chapter 3, pp. 43–96.

[4] P. Ciureanu, Magnetoresistive sensors, in: P. Ciureanu, S. Middelhoek (Eds.), Thin Film Resistive Sensors, IOP Publishers, Bristol, 1992.

[5] C. Schott, F, Burger, H. Blanchard, L. Chiesi, Modern integrated silicon Hall sensors, Sensor Review, vol. 18 (4), 1998, pp. 252–257.

[6] F. Burger, New fully integrated 3D silicon Hall sensor for precise angular position measurements, Sens. Actuators A: Phys. 67 (1–3) (1998) 72–76.

[7] C.S. Roumenin, Magnetic sensors continue to advance towards perfection, Sens. Actuators A: Phys. 46–47 (1995) 273–279.

[8] N. Mathieu, A. Chovet, M. Chertouk, Figures of merit of semiconductor integrated magnetic sensors, Sens. Mater. 5 (6) (1994) 359–368.

[9] C.H. Smith, R.W. Schneider, Magnetic filed sensing utilizing GMR materials, Sens. Rev. 18 (4) (1998) 230–236.

[10] A.E. Mahdi, D.J. Mapps, High-Tc SQUIDs: the ultra sensitive sensors for non-destructive testing and biomagnetism, Sens. Actuators A: Phys. 81 (1–3) (2000) 367–370.

[11] J.E. Lenz, A review of magnetic sensors, Proc. IEEE 78 (6) (1990) 973–989.

[12] J.M. Janicke, Second harmonic fluxgate sensors and magnetometers, Sensor Rev. 18 (4) (1998) 225–229.

[13] M.N. Baibich, J.M. Broto, A. Ferti, F.N. Van Dau, F. Oetroff, P. Eitenne, G. Creuzet, A. Friederich, J. Chazelas, Giant magnetoresistance of (001)Fe/(001)Cr magnetic superlattices, Phys. Rev. Lett. 61 (1988) 2472–2475.

[14] D.J. Mapps, Magnetoresistive sensors, Sens. Actuators A: Phys. 59 (1997) 9–19.

[15] N.M. White, J.D. Turner, Thick-film sensors: past, present and future, Meas. Sci. Technol. 8 (1997) 1–20.

[16] J. Fraden, Handbook of Modern Sensors: Physics, Designs and Applications, second ed., Springer, New York, USA, 1996, Chapter 15, pp. 444–457.

[17] H. Koch, Mature SQUID-systems and their application, IEEE Trans. Appl. Supercond. 7 (2) (1997) 3738–3743.

[18] J. Clarke, SQUIDs fundamentals, in: H. Weinstock (Ed.), SQUID Sensors: Fundamentals, Fabrication and Applications, Kluwer Academic Publishers, Dordrecht, 1996.

[19] J.P. Wikswo, SQUID magnetometers for biomagnetism and non-destructive testing: important questions and initial answers, IEEE Trans. Appl. Supercond. 5 (2) (1995) 74–120.

[20] M. Bick, K. Sternickel, G. Panaitov, A. Effern, Y. Zhang, H.-J. Krause, SQUID gradiometry for magnetocardiography using different noise cancellation techniques, IEEE Trans. Appl. Supercond. 11 (1) (2001) 673–767.

[21] R.L. Fagaly, Superconducting sensors: instruments and applications, Sensors 13 (10) (1996) 18–27.

[22] D. Cohen, E.A. Edelsack, J.E. Zimmerman, Magnetocardiograms taken inside a shielded room with a superconducting point-contact magnetometer, Appl. Phys. Lett. 16 (7) (1970) 278–280.

[23] D. Cohen, Magnetoencephalography: detecting the brain's electrical activity with a superconducting magnetometer, Science 175 (1972) 664–666.

[24] J. Clarke, SQUIDs: theory and practice, in: H. Weinstock, R.W. Ralston (Eds.), The New Superconducting Electronic, Kluwer Academic Publishers, Dordrecht, 1993.

[25] J. Clarke, R.H. Koch, The impact of high-temperature superconductivity on SQUID magnetometers, Science 242 (1988) 217–223.

[26] B. David, O. Dossel, V. Doormann, R. Eckart, W. Hoppe, J. Kruger, H. Laudan, G. Rabe, The development of a high-T_c magnetocardiography system for unshielded environment, IEEE Trans. Appl. Supercond. 7 (2) (1997) 3267–3270.

[27] H.J. Barthelmess, M. Halverscheid, B. Schiefenhovel, E. Heim, M. Schilling, R. Zimmermann, Low-noise biomagnetic measurements with a multichannel dc-SQUID system at 77 K, IEEE Trans. Appl. Supercond. 11 (1) (2001) 657–660.

[28] T. Van Duzer, Superconductor electronics: 1986–1996, IEEE Trans. Appl. Supercond. 7 (2) (1997) 98–111.

[29] A.I. Braginski, Fabrication of high-temperature SQUID magnetometers, in: H. Weinstock (Ed.), SQUID Sensors: Fundamentals, Fabrication and Applications, Kluwer Academic Publishers, Dordrecht, 1996, pp. 235–288.

[30] H.J.M. ter Brake, R. Huonker, H. Rogalla, New results in active noise compensation for magnetically shielded rooms, Meas. Sci. Technol. 4 (1993) 1370–1375.

[31] P. Seidel, F. Scmidl, R. Wiedl, S. Wunderlich, L. Dorrer, High-T_c SQUID systems for biomagnetic clinical research and for non-destructive evaluation, in: N. Koshizuka, S. Tajima (Eds.), Advances in Superconductivity XI, vol. 2, Springer, New York, pp. 1193–1198.

[32] D. Drung, Advanced SQUID read-out electronics, in: H. Weinstock (Ed.), SQUID Sensors: Fundamentals, Fabrication and Applications, Kluwer Academic Publishers, Dordrecht, 1996, pp. 63–116.
[33] R. Clem, A high-T_c superconducting magnetic sensor for detection of subsurface structures, in: Proceedings of the SPIE—the International Society for Optical Engineering, Denver, USA, vol. 3752, 1999, pp. 113–124.
[34] R.P. Hunt, A magnetoresistive readout transducer, Proc. IEEE, Trans. Magn. 7 (1) (1971).
[35] D.J. Mapps, Magnetoresistive sensors, Sens. Actuators A: Phys. A59 (1997) 9–19.
[36] Philips Semiconductors, Data Sheet: General Appendices, File under Discrete Semiconductors, SC17, January 1997.
[37] http://www.storage.ibm.com/hdd/ipl/oem/tech/eraheads.htm.
[38] D.J. Mapps, N. Fry, D. Smith, Non-Linear Magnetoresistance, Nonlinear Electromagnetic Systems, vol. 10, IOS Press, ISBN 90-5199-251-3, 1996.
[39] K. Kuijk, W. van Gesteland, F. Gorter, The barber-pole: a linear magnetoresistance head, IEEE Trans. Magn. 11 (1975) 1215–1219.
[40] D. Robbes, C. Dolabdjian, S. Saez, Y. Monfort, G. Kaiser, P. Ciureanu, Highly sensitive uncooled magnetometers: state of the art, IEEE Trans. Appl. Supercond. 11 (1) (2001) 629–634.
[41] Y.Q. Mapps, M.A. Akhter, Optimisation of material and structure for a switched-bias magnetoresistive sensor, Sens. Actuators A: Phys. 81 (2000) 60–63.
[42] D.J. Mapps, British Patent No. 2262635 (8 November 1991).
[43] M.N. Baibich, J.M. Broto, A. Fert, F.N. van Dau, F. Petroff, Giant magnetoresistance of (001) Fe/cr magnetic superlattices, Phys. Rev. Lett. 61 (1988) 2472–2475.
[44] J.C.S. Kools, Exchange-biased spin valves for magnetic storage, IEEE Trans. Magn. 32 (4) (1996) 3165–3184.
[45] E. Grochowski, Emerging trends in data storage on magnetic disk drives, Datateck Journal (Launch Edition), ICG Publishing, ISSN 1464-6021, 1999.
[46] M. Xiao, K. Laassen, J. Peppen, M. Kryder, Extralow noise in giant magnetoresistance recording heads, J. Appl. Phys. 95 (8) (1999) 5855–5857.
[47] J.S. Moodera, L.R. Kinder, T.M. Wong, R. Messervey, Large magnetoresistance at room temperature in thin-film tunnel junctions, Phys. Rev. Lett. 74 (1995) 3273–3276.
[48] M. Sato, H. Kikuchi, H. Kobayashi, Effects of interface oxidation in ferromagnetic tunnel junctions, IEEE Trans. Magn. 35 (5) (1999) 2946–2948.
[49] L.V. Panina, K. Mohri, Magneto-impedance effect in amorphous wire, Appl. Phys. Lett. 65 (1994) 1189.
[50] J. Velazquez, M. Vazquez, D.-X. Chen, A. Hernando, Giant magneto-impedance in non magnetostrictive amorphous wires, Phys. Rev. B 50 (1994) 16737.
[51] K. Mohri, T. Uchiyama, L.V. Panina, Recent advances of micro-magnetic sensors and sensing application, Sens. Actuators A 59 (1997) 1.
[52] K. Mohri, T. Kohzawa, K. Kawashima, H. Yoshida, L.V. Panina, Magneto-inductive effect in amorphous wires, IEEE Trans. Magn. 28 (1995) 3150.
[53] T. Kitoh, K. Mohri, T. Uchiyama, Asymmetrical magneto-impedance effect in twisted amorphous wires for sensitive magnetic sensors, IEEE Trans. Magn. 31 (1995) 3137.
[54] L.V. Panina, D.P. Makhnovskiy, K. Mohri, Mechanism of asymmetrical magneto-impedance in amorphous wires, J. Appl. Phys. 85 (1999) 5444–5449.
[55] T. Gunji, L.V. Panina, K. Mohri, Asymmetrical magneto-impedance effect in amorphous wires, J. Magn. Soc. Japan 21 (1997) 793.
[56] T. Uchiyama, K. Mohri, L.V. Panina, K. Furuno, Magneto-impedance in sputtered amorphous films for micro magnetic sensors, Trans. IEE Japan 19 (115-A) (1995) 949.
[57] T. Morikawa, Y. Nishibe, et al., Enhancement of giant magneto-impedance layered film by insulator separation, IEEE Trans. Magn. 32 (1996) 4965.
[58] D.P. Makhnovsky, L.V. Panina, Size effect on magneto-impedance in layered films, Sens. Actuators A: Phys. 81 (2000) 91–94.
[59] T. Kanno, K. Mohri, T. Yagi, T. Uchiyama, L.P. Shen, Amorphous wire MI micro sensor using C-MOS IC multivibrator, IEEE Trans. Magn. 33 (1997) 3358.